ELSEVIER

Journal of Materials Processing Technology 133 (2003) 218–224

Journal of Materials Processing Technology

www.elsevier.com/locate/jmatprotec

Creep mechanisms of ferritic oxide dispersion strengthened alloys

A. Wasilkowska[a,*], M. Bartsch[b], U. Messerschmidt[b], R. Herzog[c], A. Czyrska-Filemonowicz[a]

[a]*Faculty of Metallurgy and Materials Science, University of Mining and Metallurgy, al. Mickiewicza 30, PL-30-059 Krakow, Poland*
[b]*Max Planck Institute of Microstructure Physics, Weinberg 2, D-06120 Halle, Germany*
[c]*Institute for Materials and Processes in Energy Systems, Research Centre Jülich GmbH, D-52428 Jülich, Germany*

Abstract

A study of creep mechanisms of ferritic ODS alloys was based on high temperature tensile/compression tests combined with electron microscopy analysis of deformed specimens and in situ observations of dislocation motion under stress. The flow stress, its strain-rate sensitivity and its temperature dependence were discussed in terms of solid solution hardening, mutual dislocation interaction, the Orowan process, a thermally activated detachment model and solute drag effects. The mechanisms controlling the flow stress of ferritic ODS alloys were identified.

Keywords: ODS alloys; Compression; Relaxation; Creep; In situ straining; TEM; HVTEM; Incoloy MA956; PM2000

1. Introduction

Iron-based oxide dispersion strengthened (ODS) alloys exhibit a high creep strength at temperatures from 900 to 1100 °C, which is achieved by: (1) the incorporation of very fine Y–Al oxide particles in a ferritic matrix and (2) the recrystallization of the structure at 1350 °C for 1 h, leading to coarse grains with high grain aspect ratios (GARs) in the direction of stress (Fig. 1). The upper limit of the alloys service temperature follows from the dispersoids' instability at above 1100 °C [1].

The creep strength of ferritic ODS alloys combined with an excellent oxidation resistance make them promising materials for strategic power plant components [2–4]. The creep behaviour of iron-based ODS alloys has been investigated extensively on commercial products of such companies as: Inco Alloys International, UK (e.g. Incoloy MA956) and Plansee GmbH, Austria (PM2000) [4–8]. The results have lead to an improved understanding of the high temperature deformation mechanisms of dispersion strengthened alloys.

In this paper, the mechanisms responsible for the deformation behaviour of ferritic ODS alloys are discussed in correlation with the dislocation structure of steady-state deformed specimens and the dynamics of dislocation motion investigated in situ at temperatures of up to 1050 °C.

2. Material and experimental

The investigated alloys Incoloy MA956 and PM2000 were supplied as-recrystallized bars of 20 and 16 mm diameter, respectively. The alloy MA956 has a chemical composition of: 74 wt.% Fe–19.9 wt.% Cr–4.6 wt.% Al–0.38 wt.% Ti–0.51 wt.% Y–0.019 wt.% C–0.014 wt.% N–0.19 wt.% O. Table 1 shows the nominal composition of the investigated alloys in comparison with that of dispersoid-free alloy Kanthal (similar to ODS matrix) [5].

The standard longitudinally machined specimens were subjected to constant load (creep tests) or constant strain-rate (tensile tests) at temperatures of 900–1050 °C. From the creep tests, the minimum deformation rate $\dot{\varepsilon}$ was determined as a function of the applied stress σ (constant as long as the strain is below 0.2%). Tensile tests allow higher deformation rates to be applied (between 10^{-4} and 10^{-1} s^{-1}). In the latter case, the flow stress corresponding to a stress "plateau" (appearing in the tensile curve before specimen necking) is measured as a function of the constant deformation rate (equal to that applied by a machine). Deformation data were presented as plots of $\ln \dot{\varepsilon}$ vs. $\ln \sigma$. A slope of this diagram equals the stress exponent m in the Norton power-law creep equation [9].

The temperature dependence of the flow stress and its strain-rate sensitivity were determined by macroscopic compression tests including strain-rate cycling and stress relaxation experiments. Compression tests were carried out between room temperature and 900 °C under an initial strain-rate of 1×10^{-4} s^{-1}. Samples were cut from a single large grain of alloy MA956 (size 1.25 mm× 1.5 mm × 4.3 mm). The

* Corresponding author.

0924-0136/02/$ – see front matter © 2002 Published by Elsevier Science B.V.
PII: S0924-0136(02)00237-6

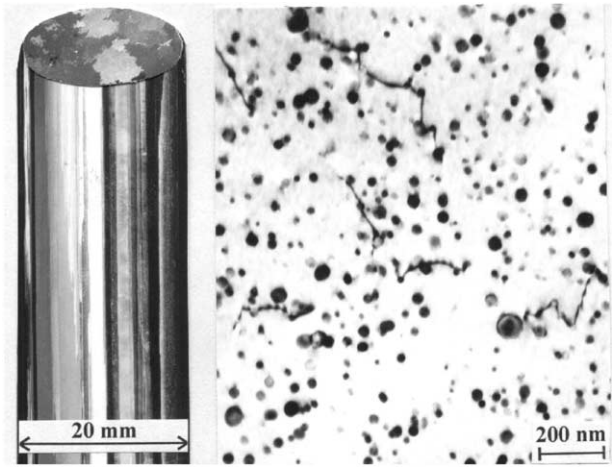

Fig. 1. The as-recrystallized ODS alloy MA956: (a) a structure of an etched bar and (b) a distribution of dispersoids in mechanically alloyed matrix.

Table 1
Nominal chemical composition of the iron-based ODS alloys investigated in comparison with the alloy Kanthal (wt.%)

Alloy	Fe	Cr	Al	Ti	Y_2O_3
MA956	Balance	20	4.5	0.5	0.5
PM2000	Balance	20	5.5	0.5	0.5
Kanthal	Balance	22	5.0	–	–

strain-rate sensitivity r equals the reciprocal slope of plots $\ln(-\dot{\sigma})$ vs. σ, where $-\dot{\sigma}$ means the negative stress rate (proportional to the plastic strain-rate $\dot{\varepsilon}$).

The in situ straining experiments were performed at room temperature and at temperatures between 640 and 1010 °C. Microtensile samples (8 mm × 2 mm × 0.1 mm) were cut longitudinally from the MA956 bar, then ground, centrally dimpled and polished using an electrolyte of 100 ml $HClO_4$ in 900 ml ethanol ($T < -20$ °C, $I = 200$ mA). The specimens were deformed in an HVTEM operated at 1 MV [10]. The dislocation shape and motion under load were recorded photographically or on video tape.

Details of microstructure analyses of the as-received alloys were published elsewhere [6,8]. The structural analysis of selected high temperature deformed samples was performed by means of transmission electron microscopy of thin foils prepared as described above. TEM investigations had been performed using JEM 2010 ARP electron microscope. For quantitative analysis of the dislocation structure, e.g. the dislocation density, Burgers vector and slip planes, a double-tilting specimen holder was used following the procedure described in [11,12].

3. The structural characteristics of ODS alloys

A typical structure of an as-recrystallized iron-based ODS alloys is shown in Fig. 1. The microstructure parameters of as-received alloys are given in Table 2 (where GAR is the grain aspect ratio, f the volume fraction of dispersoids, d the mean particle size and l the mean interparticle spacing). Both bars of MA956 and PM2000 exhibit a similar GAR, but have a different texture. The distribution of Y–Al oxide particles in the ferritic matrix was fairly homogeneous. The mean dislocation density in the as-received ODS alloys was about 1×10^{13} m/m^3. The value of the dislocation density is far higher than a typical one for annealed crystals, suggesting a pre-straining of about 10%. The reference alloy Kanthal exhibits equiaxial coarse grains of about 548 μm size [5].

Table 2
The structural characteristics of the ODS alloys investigated

Alloy	Grains		Dispersoids		
	GAR	Texture	f (%)	d (nm)	l (nm)
MA956	>30:1	⟨1 1 1⟩	1.46	24	149
PM2000	>30:1	⟨1 0 0⟩	1.06	20	137

4. Results of the high temperature deformation tests

Fig. 2 presents the plot of minimum deformation rate $\dot{\varepsilon}$ against the flow stress σ (determined from creep and high temperature tensile tests) in logarithmic scale. The data were compared with that for dispersoid-free alloy Kanthal, reported in [5]. The effect of dispersoids appeared in the decrease of the minimum creep rate by several orders of magnitude at the same applied stress. A nearly vertical drop in $\ln\dot{\varepsilon}-\ln\sigma$ plot is typical for the coarse-grained ODS alloys [3]. It enables the definition of a critical stress σ_{th} below which the creep rate is immeasurably small. As shown in

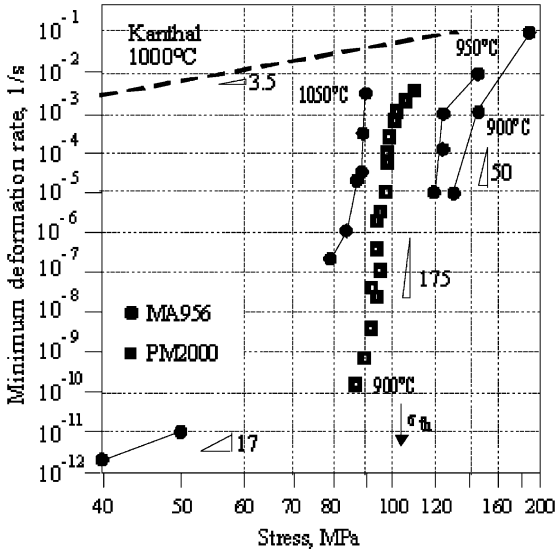

Fig. 2. Creep rate vs. stress for as-recrystallized iron-based ODS alloys and for dispersoid-free alloy Kanthal.

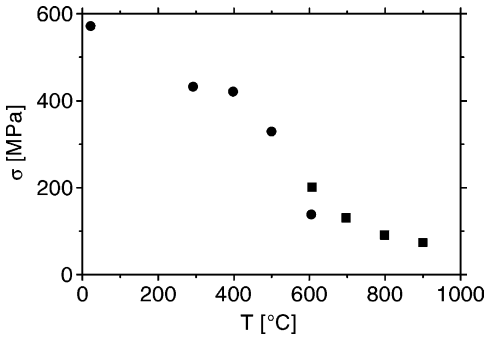

Fig. 3. Temperature dependence of the critical flow stress (data from two compression samples—circles and squares).

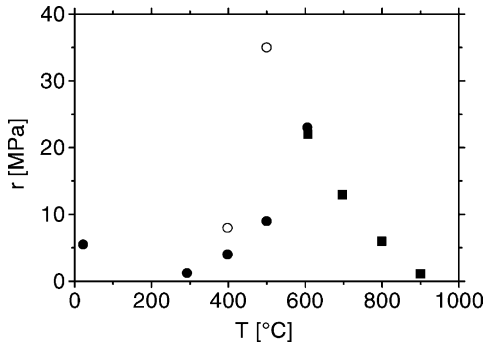

Fig. 5. Temperature dependence of the strain-rate sensitivity of stress r (full symbols correspond to the initial relaxation rates, open symbols to the intermediate).

Fig. 2, at high temperatures and very low stresses, $\dot{\varepsilon}$ decreases more gradually with σ, indicating a change in the rate-controlling processes. Raj [3] shows for various ODS alloys that at low temperatures and high stresses the $\ln\dot{\varepsilon}-\ln\sigma$ slope tends to follow that of the dispersoid-free alloy Kanthal, with stress exponents m of about 3–5 (typical for the dislocation creep of pure metals and alloys).

The results obtained at 900 °C and strain-rates of above $10^{-5}\,s^{-1}$ revealed that the tensile strength of alloy with ⟨1 1 1⟩ texture (Incoloy MA956) is about 30% higher than that of an alloy with ⟨1 0 0⟩ texture (PM2000). As mentioned in [6], the influence of texture on the high temperature strength of ODS alloys can be assigned to different Schmidt factors.

Experimental compression curves of single crystal MA956 specimens show weak work hardening during compression, more pronounced at 300 °C, and yield-drop effects at 600 and 700 °C. In Fig. 3, the dependence of the flow stress σ on the applied temperature T is presented. The plot shows an initial decrease of the flow stress above room temperature, than a "plateau" at temperatures of about 300–400 °C and further decrease at higher temperatures. A similar $\sigma(T)$ dependence was found by Dubiel et al. [13] and by Lee [5] (PM2000, Kanthal). The values of the flow stress measured under compression are lower than those determined in tension [13].

Results of the stress relaxation tests are plotted as $\ln(-\dot{\sigma})$ vs. σ for different temperatures and an initial strain-rate of $10^{-4}\,s^{-1}$ (Fig. 4). "Relaxation" means the stress drop due to the machine stop, resulting only in the plastic deformation of sample by gliding. At temperature of 23 °C the plot was linear. The experimental curve obtained at about 300 °C was very steep. At 500 °C, the relaxation curve exhibited a steep part in the beginning of the experiment, however, for intermediate relaxation rates an increasing strain-rate sensitivity of stress r with decreasing strain-rate was observed ("inverse" curvature). At a temperature of about 700 °C the plot showed the "usual" curvature—decreasing $r = \Delta\sigma/\Delta\ln(-\dot{\sigma})$ with decreasing strain-rate $\dot{\varepsilon}$.

The temperature dependence of the strain-rate sensitivity of the flow stress is presented in Fig. 5. Full symbols represent r values determined in the beginning of each relaxation curve. Open symbols represent r values for intermediate relaxation rates. The decreasing strain-rate sensitivity of stress ($r=5.5$ MPa at 23 °C and $r=1.2$ MPa at 300 °C) was detected. In the beginning of the relaxation test r exhibited a maximum at about 600 °C and decreased afterwards up to 900 °C to a very small value. For intermediate relaxation rates the strain-rate sensitivity of the stress shows a strong maximum at about 500 °C.

The temperature dependence of the stress exponent m, defined as the slope of $\ln\dot{\varepsilon}$ vs. $\ln\sigma$ ($m=\sigma/r$) is plotted in Fig. 6 for a strain-rate of $10^{-4}\,s^{-1}$. It initially increases, but then exhibits a strong drop between 300 and 600 °C. Above 600 °C the stress exponent slowly increases to a value of $m = 70$ at 900 °C. At lower strain-rates ($\dot{\varepsilon} \leq 10^{-6}\,s^{-1}$) and

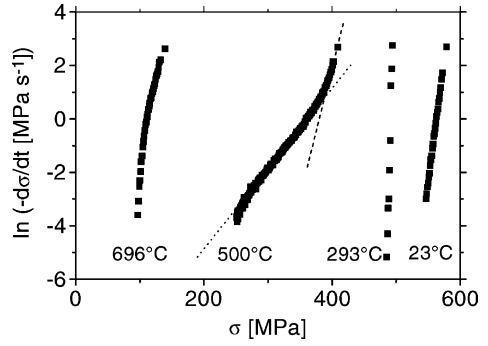

Fig. 4. Stress relaxation curves obtained for temperatures between 23 and 700 °C.

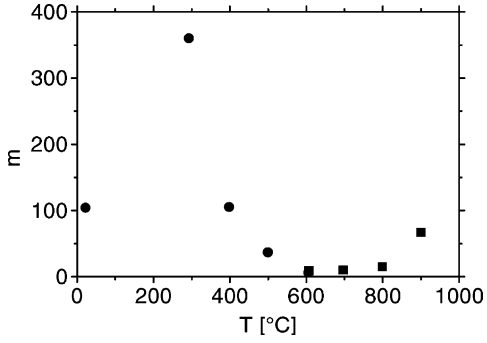

Fig. 6. Temperature dependence of the stress exponent m.

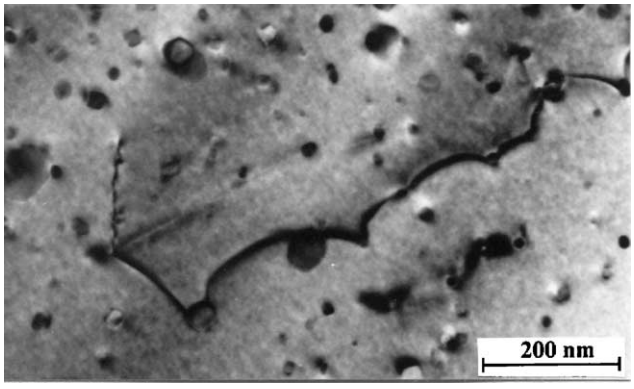

Fig. 7. Pinning of dislocations at the particle–matrix interface.

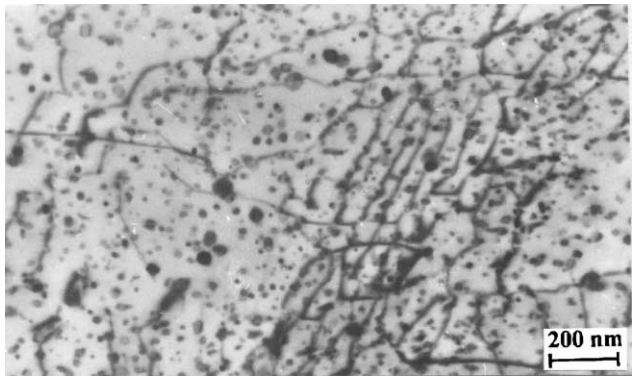

Fig. 9. Collective arrangement of dislocations.

temperatures between 900 and 1200 °C, the stress exponent decreases with the temperature [6].

5. Dislocations in deformed ferritic ODS alloys and their motion under high temperature straining

To understand the deformation mechanisms responsible for the creep behaviour of iron-based ODS alloys it was useful to correlate the slope changes in Fig. 2 directly with the microstructure of the specimens. Thus, selected specimens of alloys MA956 and PM2000 were investigated in their homogeneous deformed volume (far from the necking).

At all temperatures and stresses the particular interaction of dislocations with the incoherent interface of dispersoids was observed, suggesting the Rösler–Arzt mechanism [14] being responsible for the creep rate (Fig. 7).

At stresses close to the critical value (which is a function of temperature and alloy structure; e.g. for PM2000 at 900 °C: $\sigma_{th} = 108$ MPa), the dislocation structure was characterized by single dislocations of mean density at about 2×10^{13} m/m^3. No subgrains were detected, probably due to the small strain in the secondary creep region, usually less than 0.2%.

The observation of fragmentary subgrain formation was limited to temperatures below 950 °C and stresses higher than the critical value (Fig. 8). The density of free dislocations increased up to 3×10^{13} m/m^3. In this stress/temperature range the coupling between climbing of dislocations, dislocation detachment and solid solution strengthening is expected, which leads to a more gradually decrease in the steady-state deformation rate with the stress. The respective model is described in [6].

At higher temperatures (1050 °C) and very low stresses (40–50 MPa) the dislocations were bound to the particles in local groups. The collective arrangement of dislocations (Fig. 9) suggests that deformation probably proceeds through the "easy path" of particle structure, related to the random distribution of dispersoids in the alloy matrix. A collective dislocation motion was also observed in situ at 1010 °C.

In situ straining experiments of a ferritic ODS alloy Incoloy MA956 allowed for a direct observation of dislocation motion inside a field of particles. The Burgers vector coincides with $(1/2)\langle 1\,1\,1\rangle$ lattice vector of the b.c.c. matrix. Dislocations move jerkily between dispersoids when the deformation temperature amounts to 23 °C (slip plane {1 1 0}) or at temperatures above 750 °C (in all planes containing the Burgers vector, i.e. {1 1 0}, {1 1 2} and {1 2 3}).

At temperatures of 650–750 °C, the dislocations change their mode of motion to the viscous one. The pinning of smoothly curved dislocations at the oxide particles was observed (Fig. 10), however, the main effect of dispersoids

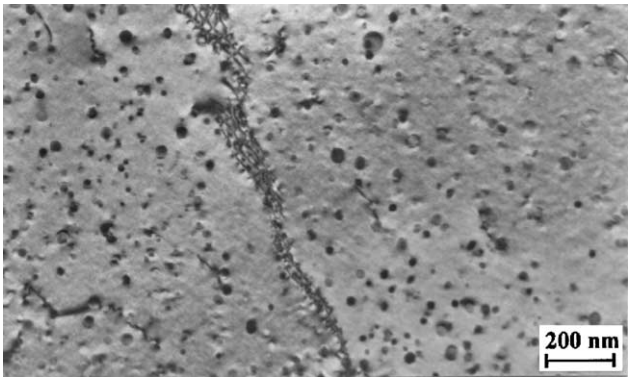

Fig. 8. A fragmentary creation of a subgrain boundary.

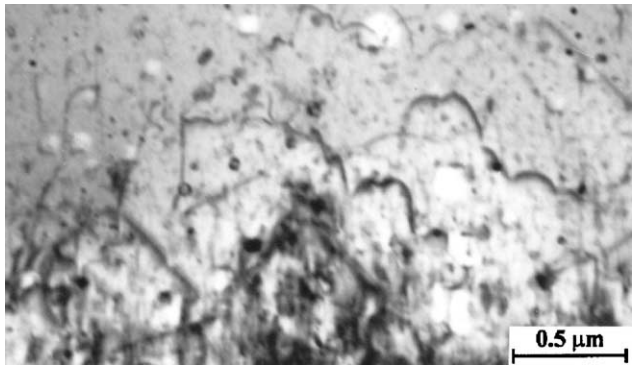

Fig. 10. In situ observation of dislocation shape under loading.

seemed to be the temporary reduction of the velocity of dislocation viscous glide owing to the back stress acting on the segments bowing-out between particles [15]. The measured effective distances between pinning points is larger than calculated from the dispersoid size and distribution, and amounts to 220 nm. This result points to the existence of particle strength distribution for the moving dislocations.

6. Discussion of the high temperature deformation mechanisms of ferritic ODS alloys

The resistance of obstacles to dislocation motion determines the flow stress of alloys at high temperatures. The various kinds of barriers may affect the dislocation motion in ODS alloys, e.g. solute atoms, the own line tension of bowed-out dislocation, cutting and passing of other dislocations or overcoming of particles [16]. The flow stress is given by the sum of:

(i) an athermal stress:

$$\tau_i = \alpha\mu b\sqrt{\rho} \tag{1}$$

where ρ is the dislocation density, μ the shear module, and α is a constant depending on the dislocation arrangement; and

(ii) an effective stress:

$$\tau_e = \frac{U_0 - kT\ln(\dot{\gamma}_0/\dot{\gamma})}{V_a} \tag{2}$$

where U_0 is the activation energy, k the Boltzmann constant, T the absolute temperature, $\dot{\gamma}$ the strain-rate, and V_a the activation volume.

While the effective stress τ_e works on the thermally activated motion of dislocations, the athermal stress τ_i (the so-called internal stress) arises from the mutual dislocation interaction [16]. The separation of both stresses allows the obstacles for dislocation motion to be identified.

As shown in Fig. 3, at low temperatures (a region between 23 and 300 °C) and at high temperatures (above 400 °C), the flow stress decreases with the increase of temperature, thus indicating a thermally activated deformation process. At the intermediate temperatures (300–400 °C) the flow stress is almost independent of the temperature, indicating $\tau_e = 0$.

It was observed during in situ straining, that the behaviour of dislocation motion is different depending on whether the effective stress exists or not. When the effective stress can be considered as absent, dislocations move very quickly after surmounting of the internal stress peak. On the other hand, when a significant effective stress exists, dislocations move viscously. The absence or presence of effective stress reflects also the change of the stress relaxation rate (Fig. 4). At intermediate temperatures (400–500 °C), the strain-rate dependence of the flow stress is inverse of that usually observed. Further, the stress exponent m decreases sharply with temperature (Fig. 6).

The above deformation behaviour can be explained by considering the interaction between solute atoms and dislocations. At low temperatures, the solute atoms hinder the dislocation motion as steady obstacles. The interaction energy ΔG° is proportional to the atom size misfit δ [17]:

$$\Delta G^\circ \cong \mu b^3 \delta \tag{3}$$

A rough estimation using the above equation with an usual value of $\delta = 0.1$ and $\mu \cong 60$ GPa yields $\Delta G^\circ \cong 0.6$ eV. Such a small value of interaction energy means a negligible solution strengthening effect at high temperatures. However, solutes can be responsible for a flow stress increase of about 150 MPa when the temperature decreases from 300 °C down to room temperature (Fig. 3). From the jerky motion of dislocations observed at room temperature, follows that this part is not large.

In order to explain the inverse strain-rate dependence of the flow stress at temperatures of around 400–600 °C, it can be suggested that obstacles to dislocation motion are formed by a thermally activated process [16]. At high temperatures, solute atoms diffuse preferentially to places of low interaction energy with dislocations, and asymmetric atmospheres with various concentrations may be formed around a moving dislocation. The dislocation experiences a friction force proportional to its velocity of glide. The atmosphere acts against the glide and against the climb of dislocations also, causing a viscous dislocation motion.

The existence of a flow stress ''plateau'' between about 300–400 °C in Fig. 3 ($\Delta\sigma/\Delta T = 0$) suggests that athermal obstacles, e.g. the long-range stress field of other dislocations and/or strong dispersing particles, control the flow stress of alloy MA956. The internal stress τ_i was calculated using Eq. (1) for Taylor hardening. For a first estimation, α is taken to be equal to 0.5; the shear modulus $\mu \cong 60$ GPa at room temperature and 30 GPa at 880 °C [15]. The dislocation densities in high temperature deformed specimens were measured to be of the order of 2×10^{13} m/m^3. Thus, the calculated value of shear stress at 880 °C is $\tau_i \cong 24$ MPa.

The internal shear stress was compared with the compressive flow stress via the relationship $\tau = M\sigma$, where M is the Taylor factor set equal to 0.4, as that for single crystals. The results showed that a long-range mutual dislocation interaction may contribute to the critical flow stress at room temperature (at least of the order of $\sigma_i \cong 100$ MPa) and is essential also at high temperatures.

A critical shear stress at which dislocations can glide through the obstacles at a temperature of absolute zero is given by the Orowan stress, here expressed by the Scattergood and Bacon equation [18]:

$$\tau_{Or} = \frac{2K}{b(l-d)}\left\{\ln\left(\frac{X}{b}\right) + 0.7\right\} \tag{4}$$

The Orowan stress of a screw dislocation K means the prelogarithmic factor of the edge dislocation line energy (and vice versa). The length parameter X for small particles is

almost equal to the particle diameter d (24 nm). In Eq. (4), the effective interparticle distance determined by in situ tests of $l = 220$ nm was used. It is slightly larger than the mean value of 150 nm, implying that only a fraction of the particles impede the dislocation motion effectively. Taking, additionally, into account the random arrangement of the particles the correction factor of 0.84 in the Orowan stress gives values about 40% smaller, i.e. $\sigma_i \cong 210$ MPa at room temperature and 120 MPa at 880 °C. These values should be considered as the upper limits of the Orowan stress.

In the case of the Orowan process, the temperature dependence of the flow stress is only due to the temperature dependence of the dislocation energy K in Eq. (4). It was shown in [15] that above 700 °C the flow stress depends more strongly on the temperature than is predicted by the Orowan mechanism. The back stress τ_b (estimated on individual dislocation loops by computer simulation of their shape under stress) was only 27% of the average Orowan stress at a temperature of 700 °C. The reason may be in the operation of a thermally activated mechanism, e.g. Peierls potential, point defect drag or, for instance, detachment of dislocations from the pinning obstacles (the R–A model).

According to the model of Rösler and Arzt [14], after overcoming the dispersoids, dislocations remain attached at the particle–matrix interface. In order to contribute to the deformation, it is necessary to release them from the pinning dispersoids. In the athermal case, the stress for detachment of the dislocations from the particles is given by

$$\tau_d = \sqrt{1 - k^2}\tau_{Or} \tag{5}$$

where k is a parameter describing the relaxation of the stress field of the dislocation at the particle surface.

At finite temperatures, the dislocations can detach from the particles at stresses lower than τ_d. They spend most of their time at the departure side of the particles waiting for thermally activated detachment so that this process controls the average dislocation velocity during alloy deformation. The stress exponent in the R–A model can be expressed as

$$m = \frac{3}{2}\frac{Gb^2 r}{kT}(1-k)^{3/2}\left(1 - \frac{\tau}{\tau_d}\right)^{1/2}\frac{\tau}{\tau_d} \tag{6}$$

Gb^2 is a line tension of dislocation, for a rough estimation equal to 3×10^{-10} N. The experimentally fitted $k = 0.66$ [6]. The term $(1 - \tau/\tau_d)^{1/2}(\tau/\tau_d)$ varies only slowly with stress and can be approximated by 0.35. With these data, the theoretical value of m turns out to be quite large (about $m = 100$ at 700 °C) and to decrease with increasing temperature. The experimental data in Fig. 6, where $m \cong 10$ at 700 °C and increases with temperature, shows that at temperatures between 700 and 900 °C and strain-rates of 10^{-4} s^{-1}, the "thermally activated detachment" is no longer controlling the deformation process. The predictions of the R–A model are in good agreement with creep test results only for stresses near to the critical stress [6]. Thus, a thermally activated detachment of dislocations from oxide particles can be a proper mechanism explaining the existence of a threshold stress for creep in ODS alloys.

7. Conclusions

A number of factors appear to influence the creep behaviour of coarse-grain ferritic ODS alloys, e.g. texture, particle distribution, the range of stresses and temperatures. The quantitative description of dislocation dynamics supported by macroscopic compression and stress relaxation tests lead to the following conclusions:

1. The solid solution hardening can be an essential strengthening mechanism at low temperatures, close to room temperature.
2. At temperatures between 300 and 400 °C, the joint action of mutual dislocation interactions and the Orowan mechanism are seen to be the governing deformation mechanisms.
3. The dragging of solutes atmospheres may result in the viscous dislocation motion and in the maximum strain-rate sensitivity of the stress at intermediate temperatures.
4. The importance of oxide dispersions becomes relevant at higher temperatures (above 900 °C), when a pinning of dislocations by oxide particles leads to an effective strengthening, compared to the dispersoid-free alloy Kanthal. At stresses higher than the critical value, the long-range interaction between dislocations might be an important deformation mechanism again.

Acknowledgements

This study was supported by the University of Mining and Metallurgy, project no. 10.10.110.31. The authors are grateful to Dr. Dietmar Baither for making available his PC programmes for calculating the dislocation line energy.

References

[1] H.E. Cama, The effect of high temperature exposure on the second phase particle populations in mechanically alloyed ferritic oxide dispersion strengthened alloys, Ph.D. Thesis, University of Leeds, Leeds, UK, 1994.
[2] F.H. Froes, J.J. de Barbadillo (Eds.), Structural Application of Mechanical Alloying, South Carolina, Myrle Beach, 1990.
[3] S. Ochiai (Ed.), Mechanical Properties of Metallic Composites, Marcel Dekker, New York, 1994.
[4] D. Coutsouradis (Ed.), Materials for Advanced Power Engineering, Kluwer Academic Publishers, Dordrecht, 1994.
[5] J.-H. Lee, Mikromechanische modellierung des kriech-verhaltens der ferritichen oxiddispersiongehärteten eisen-basissuperlegierung PM2000, Ph.D. Thesis, Universität Erlangen-Nürnberg, Germany, 1994.

[6] R. Herzog, Mikrostruktur und mechanische eigenschaften der eisenbasis-ODS-legierung PM2000, Ph.D. Thesis, RWTH Aachen, Germany, 1997.
[7] M. Weiße, Verformungsverhalten und mikrostruktur einer oxiddispersionsgehärteten eisenbasislegierung, Ph.D. Thesis, Universität Erlangen-Nürnberg, Germany, 1997.
[8] A. Wasilkowska, Żarowytrzymałość i żaroodporność stopów ODS—korelacja własności ze zmianami mikrostruktury, Ph.D. Thesis, AGH Kraków, Poland, 1998.
[9] A.K. Mukherjee, J.E. Bird, J.E. Dorn, Trans. Am. Soc. Met. 62 (1969) 155.
[10] U. Messerschmidt, M. Batsch, Ultramicroscopy 56 (1994) 163.
[11] S. Amelinckx, R. Gevers, G. Nihoul (Eds.), Defects in Crystalline Solids, Vol. 7, North-Holland, Amsterdam, 1973.
[12] A. Wasilkowska, B. Dubiel, A. Czyrska-Filemonowicz, in: Proceedings of the XVII Conference on Applied Crystallography, World Scientific, Singapore, 1998, p. 475.
[13] B. Dubiel, M. Wróbel, P.J. Ennis, A. Czyrska-Filemonowicz, Scripta Mater. 37 (1997) 1215.
[14] J. Rösler, E. Arzt, Acta Metall. 38 (1990) 671.
[15] M. Bartsch, A. Wasilkowska, A. Czyrska-Filemonowicz, U. Messerschmidt, Mater. Sci. Eng. A, in press.
[16] T. Suzuki, S. Takeuchi, H. Yoshinaga, Dislocation Dynamics and Plasticity, Springer, Berlin, 1991.
[17] F.R.N. Nabarro (Ed.), Dislocations in Solids, Vol. 4, North-Holland, Amsterdam, 1997, p. 155.
[18] R.O. Scattergood, D.J. Bacon, Philos. Mag. 31 (1975) 179.